

# MoRe: Motion-aware Feed-forward 4D Reconstruction Transformer

Juntou Fang<sup>1\*</sup>, Zequn Chen<sup>2\*</sup>, Weiqi Zhang<sup>1\*</sup>,  
 Donglin Di<sup>2</sup>, Xuancheng Zhang<sup>1,2</sup>, Chengmin Yang<sup>2</sup>, Yu-Shen Liu<sup>1†</sup>  
<sup>1</sup>School of Software, Tsinghua University, Beijing, China    <sup>2</sup>Li Auto

fangjt21@mails.tsinghua.edu.cn, chenzequn@lixiang.com, zwq23@mails.tsinghua.edu.cn  
 {didonglin, zhangxuancheng, yangchengmin}@lixiang.com, liuyushen@tsinghua.edu.cn



Figure 1. We propose MoRe, a motion-aware 4D reconstruction transformer that explicitly disentangles dynamic motion from static scene structure. This capability is enabled by our attention-forcing training strategy, which guides the model to separate motion cues from background geometry. At inference time, MoRe further supports streaming inputs through its grouped causal attention design.

## Abstract

Reconstructing dynamic 4D scenes remains challenging due to the presence of moving objects that corrupt camera pose estimation. Existing optimization methods alleviate this issue with additional supervision, but they are mostly computationally expensive and impractical in real-time ap-

plications. To address these limitations, we propose MoRe, a feedforward 4D reconstruction network that efficiently recovers dynamic 3D scenes from monocular videos. Built upon a strong static reconstruction backbone, MoRe employs an attention-forcing strategy to disentangle dynamic motion from static structure. To further enhance robustness, we fine-tune the model on large-scale, diverse datasets encompassing both dynamic and static scenes. Moreover, our grouped causal attention captures temporal dependencies and adapts to varying token lengths across frames, ensuring temporally coherent geometry reconstruction. Extensive experiments on multiple benchmarks demonstrate that MoRe

\*Equal contribution, where Zequn leads this project.

†The corresponding author is Yu-Shen Liu. This work was partially supported by Deep Earth Probe and Mineral Resources Exploration—National Science and Technology Major Project (2024ZD1003405), and the National Natural Science Foundation of China (62272263).

achieves high-quality dynamic reconstructions with exceptional efficiency. Project page: <https://hellexf.github.io/MoRe/>.

## 1. Introduction

Reconstructing the evolving three-dimensional structure of a scene (i.e., 4D reconstruction) is increasingly central to applications in augmented reality, robotics, digital twins, and immersive content creation [54, 55, 57, 58]. Classical geometry based techniques such as SfM/MVS [10, 32] and SLAM [6, 24, 36] have laid the foundation by estimating camera poses and scene structure under the assumption of a mostly static environment. They achieve high accuracy in controlled settings but struggle when objects deform or move, or when the camera undergoes complex motion.

Recent deep learning methods promise faster and more generalizable reconstruction [7, 8, 11, 16, 26, 39, 41, 46, 48, 53, 58, 59]. They split broadly into real time inference models and hybrid optimization pipelines. Real time reconstruction models map image sequences directly to camera poses and depths (or point clouds) in one feedforward pass, enabling fast processing of video input. However, these approaches are trained predominantly on static scenes. The presence of moving objects or large camera motion can significantly degrade the accuracy of estimated 3D structure. Hybrid optimization pipelines [19, 38, 47, 50] integrate learned modules such as depth estimation, optical flow estimation, or motion segmentation. However, they retain a multistage structure or rely on iterative refinement. These methods handle dynamic scenes more robustly but incur high computational cost and struggle when processing long sequences or streaming video data in real time.

A clear gap remains: how to design a fast, generalizable framework that handles camera and object motion in dynamic scenes under streaming or long sequence input while producing accurate camera poses and depths for point cloud reconstruction. We propose MoRe, a motion aware 4D streaming reconstruction system for monocular video. Our core innovation lies in teaching the reconstruction model to distinguish dynamic objects from the static background purely through training, without introducing explicit motion or segmentation priors during inference. MoRe builds upon a strong reconstruction backbone and introduces an attention forcing strategy that explicitly supervises motion disentanglement while implicitly preserving geometric consistency. This integration allows the network to learn how motion influences both scene structure and camera trajectory, enabling robust depth and pose estimation even under significant dynamic movement.

To enhance temporal coherence and scalability, we propose a temporally aware streaming inference strategy combining grouped causal attention with a bundle adjust-

ment [13] like incremental refinement process. The attention mechanism captures long range temporal dependencies and adapts to varying token lengths across frames. The refinement process incrementally updates camera poses and scene geometry to maintain temporal consistency. Combined with large scale finetuning on diverse static and dynamic datasets, MoRe achieves fast, motion aware, and generalizable 4D reconstruction suitable for real world dynamic environments.

We train our model end to end on large scale 3D datasets covering diverse static and dynamic scenarios and comprehensively evaluate its performance across multiple downstream applications. Our main contributions are as follows:

- We present MoRe, a unified motion aware 4D reconstruction framework capable of jointly estimating camera poses, depths, and motion masks in dynamic scenes.
- We introduce an attention forcing strategy that effectively teaches the network to disentangle dynamic motion from static structure during training through explicit supervision and implicit geometric consistency.
- We design a temporally aware inference mechanism combining grouped causal attention and bundle adjustment like streaming refinement, which captures long range dependencies while performing lightweight global refinement.
- Extensive experiments on diverse benchmarks demonstrate that MoRe achieves state of the art accuracy and strong generalization in dynamic 4D reconstruction.

## 2. Related Work

### 2.1. 4D Reconstruction

4D reconstruction recovers time-evolving 3D structures by jointly predicting camera poses and depth. Optimization-based systems [19, 47] refine geometry and motion using auxiliary cues (e.g., optical flow, masks), but are computationally heavy for long sequences or streaming input. Recent modular pipelines [22, 50] leverage foundation models yet remain complex for real-time use. Another line of work [9, 14, 34, 51] regresses temporally aligned point-maps; however, they often lack explicit motion-static disentanglement and require dense 4D supervision. Unlike these, MoRe preserves an elegant, easy-to-use feed-forward architecture while removing the need for auxiliary motion priors or extra annotations: we teach the model to separate dynamic and static regions during training so that inference remains lightweight, end-to-end and suitable for streaming video.

### 2.2. Learning-based Reconstruction

Recent learning-based methods directly regress geometry from images. Dust3R [41] formulates reconstruction as point-map regression, eliminating explicit calibration. Sub-

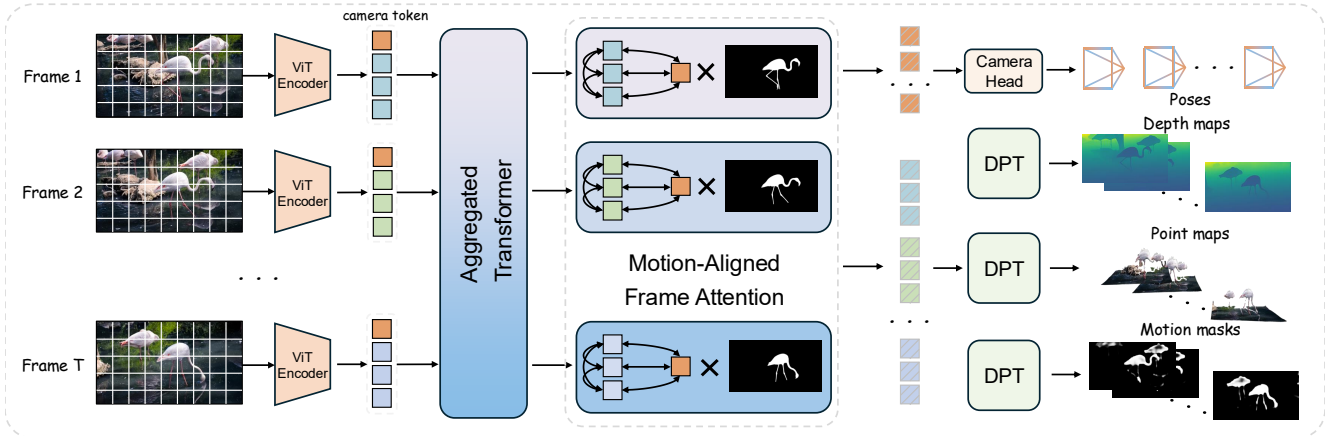


Figure 2. **Method Overview.** During training, an attention-forcing mechanism aligns the attention weights with ground-truth motion masks, enabling the model to effectively disentangle dynamic motion from static scene structure. For streaming reconstruction task, MoRe is based on a causal transformer where global attention is replaced by aggregated causal attention.

sequent works like MAST3R [18] and Fast3R [46] improve correspondences and scalability, while VGGT [39] uses a large Transformer to infer poses and depth maps across many views. Despite these advances, Transformer-based solutions face two limitations: quadratic inference costs with respect to sequence length, making streaming impractical, and a lack of explicit motion modeling, which reduces robustness in dynamic scenes. Despite their advances, Transformer-based solutions still face two key limitations: inference cost often scales quadratically with input length (making long or streaming video sequences impractical), and they typically neglect explicit modelling of camera or scene motion—which reduces robustness when objects or the camera itself move significantly. Our method addresses these shortcomings by introducing a causal attention mechanism and a streaming inference strategy, enabling efficient long-sequence processing and motion-aware geometry estimation.

### 2.3. Streaming Reconstruction

Streaming reconstruction in dynamic scenes builds on visual SLAM, which estimates trajectories and maps incrementally. However, SLAM typically assumes static environments, limiting its 4D applicability. Recent frameworks like CUT3R [40] introduce transformer-based persistent latent states for online dense reconstruction. Following this, several systems [17, 20, 61] adopt LLM-style architectures [2, 37] and unidirectional causal attention with KV-caching to handle long sequences. However, standard LLM causal attention in 3D reconstruction faces two issues: first, it breaks intra-frame token correspondences by treating tokens as a flat sequence; second, streaming input imposes hard constraints where errors accumulate and long-term context drift persists. In contrast, our method integrates a causal attention mechanism tailored for image-

tokens, combined with a BA-like token aggregation mechanism for global refinement.

## 3. Method

To address disconnections in 4D reconstruction, we propose MoRe, a feed-forward transformer designed for streaming input with a BA-like global alignment module. As shown in Fig. 2, MoRe jointly predicts per-frame depths, camera poses, point maps, and motion masks from monocular video. Our approach is built upon a formal problem formulation (Sec. 3.1), followed by an attention-forcing strategy (Sec. 3.2) that integrates implicit and explicit supervision for temporal consistency. For efficient inference, we introduce a frame-aware grouped causal attention mechanism (Sec. 3.3) tailored for streaming reconstruction, with the overall training objective detailed in Sec. 3.4.

### 3.1. Problem Formulation

Given a monocular video consisting of a frame sequence  $\{I_t \in \mathbb{R}^{3 \times H \times W}\}_{t=1}^T$ , our objective is to jointly estimate the per-frame depths  $\{D_t \in \mathbb{R}^{H \times W}\}_{t=1}^T$ , camera parameters  $\{g_t \in \mathbb{R}^9\}_{t=1}^T$ , and dynamic point maps  $\{P_t \in \mathbb{R}^{3 \times H \times W}\}_{t=1}^T$ .

4D reconstruction typically involves long temporal sequences that arrive continuously and must be processed in real time. To accommodate this streaming nature, we reformulate the task as an online process:

$$\{D_t, g_t, P_t\}_{t=1}^T = f_\theta(\{C_t\}_{t=1}^{T-1}, I_{T-1}), \quad (1)$$

where  $C_t$  represents the cached information for  $I_t$ .

Yet, streaming reconstruction further amplifies the uncertainty introduced by dynamic regions, where object motion leads to inconsistent geometry and appearance over time. The priors used in existing approaches are mainly effective in static areas and tend to fail in dynamic ones.

To address this issue, we introduce motion masks  $M_{t=1}^T$  as auxiliary guidance for motion-aware reconstruction:

$$\{D_t, g_t, P_t, M_t\}_{t=1}^T = f_\theta(\{C_t\}_{t=1}^{T-1}, I_{T-1}). \quad (2)$$

Notably, our method does not rely on motion masks as explicit inputs, since their ground truth is typically unavailable; instead, motion cues are implicitly inferred and integrated into the model’s representation.

Building upon this formulation, we next describe how our attention-forcing strategy enables MoRe to effectively exploit temporal dependencies while remaining robust to motion-induced ambiguities.

### 3.2. Motion-aligned Attention

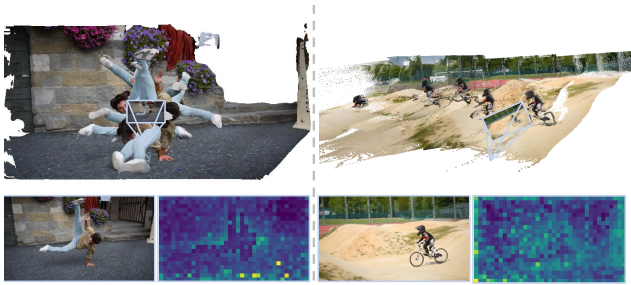


Figure 3. **Attention Map Visualization.** We visualize the attention map of the camera token within VGGT [39] and observe that the model tends to confuse moving objects with static background regions, which accounts for the degradation in prediction accuracy.

In this section, we describe how our model disentangles dynamic motion from static structure. The key strategy relies on ground-truth motion masks during training and is completely test-time-free, avoiding any additional overhead during inference.

Our motivation comes from directly transferring the foundation model to 4D reconstruction. As illustrated in Fig. 3, VGGT [39] performs well on the left example, where the camera token largely ignores moving regions. In contrast, in the right example, the camera token distributes nearly uniform attention across the image, indicating motion-induced confusion. When dynamic objects appear within an otherwise static scene, features used for camera estimation are severely corrupted, leading to degraded performance. This observation motivates the design of *motion-aligned attention*, which explicitly guides the model to focus on static regions while partially ignoring moving objects.

Motion-aligned attention is implemented by leveraging ground-truth motion masks during training. Given a motion mask  $M_t$ , we divide it into patches of size  $s \times s$  consistent with image tokenization, producing mask tokens  $\{m_i\}_{i=1}^{\frac{H}{s} \times \frac{W}{s}}$ . The motion score for each image token is computed via average pooling over its corresponding mask to-

ken:

$$a_i = 1 - \frac{1}{s^2} \sum_{(u,v) \in m_i} m_i(u,v), \quad (3)$$

where  $a_i \in [0, 1]$  represents the prior we have for image token  $i$ , with higher values corresponding to static regions. These motion scores provide a soft supervision signal, allowing the model to learn which regions should contribute more to camera estimation.

Crucially, the camera token’s attention weights  $\{\alpha_i\}$  over the image tokens can be interpreted as a probability distribution. Specifically,  $a_i$  serves as a penalty prior to modulate the distribution of  $\alpha_i$ . By supervising  $\alpha_i$  based on  $a_i$ , we provide *explicit supervision* that guides the model to differentiate between static and dynamic regions, thereby improving robustness to motion. By relying solely on ground-truth masks during training, this method avoids introducing extra outputs or computations during inference, making it fully test-time-free and suitable for streaming or real-time 4D reconstruction scenarios.

Overall, motion-aligned attention allows the model to selectively attend to informative static regions, mitigating the negative impact of dynamic objects and enabling more accurate and stable camera and scene reconstruction in challenging dynamic environments.

### 3.3. Grouped Causal Attention

In this section, we mainly discuss the streaming inference mechanism that allows MoRe to incrementally reconstruct 4D scenes in real time, based on a specially designed *grouped causal attention* scheme.

Causal attention has been widely adopted in large language models to enforce autoregressive dependency across tokens, ensuring that each token only attends to its past context. However, such a formulation is not directly suitable for our image-based reconstruction scenario. Image tokens within the same frame should maintain mutual visibility to preserve spatial coherence and consistent geometric reasoning. Therefore, we reformulate the conventional upper-triangular causal mask into a frame-wise causal mask, as illustrated in Figure, which enforces temporal causality across frames while allowing full bidirectional attention within each frame. This adaptation enables MoRe to simultaneously maintain causal temporal reasoning and spatial consistency.

During streaming inference, the first image pair initializes the key-value (KV) cache. For each subsequent frame  $I_t$ , MoRe performs causal attention over the accumulated context from previous frames:

$$F_t = \text{Attn}(\mathbf{Q}_t, [\mathbf{K}_{1:t-1}, \mathbf{K}_t], [\mathbf{V}_{1:t-1}, \mathbf{V}_t]), \quad (4)$$

$$\text{KV}_{1:t} \leftarrow [\text{KV}_{1:t-1}; (\mathbf{K}_t, \mathbf{V}_t)],$$

Here,  $F_t$  denotes the extracted feature representation for frame  $I_t$ , and  $\text{KV}_{1:t}$  stores all key-value pairs up to time

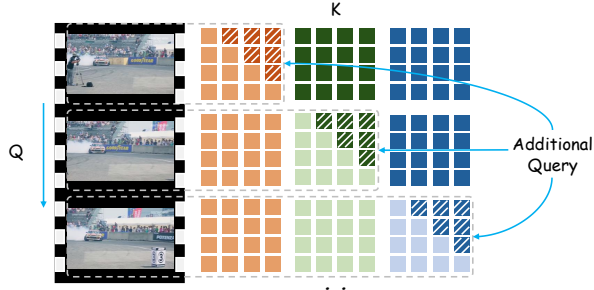


Figure 4. **Grouped Causal Attention.** Unlike traditional causal attention, our design allows image tokens within the same frame to attend to each other regardless of their ordering. This formulation enables the model to preserve causal temporal reasoning while maintaining spatial consistency within each frame.

$t$ . This design enables MoRe to process frames sequentially while preserving temporal causality and avoiding redundant recomputation, leading to highly efficient streaming 4D reconstruction.

However, such a strictly causal formulation also introduces a limitation: since each camera token only attends to its current and past contexts, long-term global information exchange becomes restricted. As a result, the accuracy of camera pose estimation may gradually degrade across extended sequences. To address this issue, we introduce a *bundle-adjustment-like token aggregation* mechanism, which serves as a lightweight post-hoc refinement step after the streaming inference.

Specifically, we cache the camera queries  $\mathbf{Q}_t^{\text{cam}}$  during inference alongside the key-value features of all frames. Once the full sequence has been processed, each camera token performs an additional attention pass over all cached features to recover global geometric consistency:

$$\mathbf{C}_t^{\text{opt}} = \text{Attn}(\mathbf{Q}_t^{\text{cam}}, [\mathbf{K}_{1:T}], [\mathbf{V}_{1:T}]), \quad (5)$$

This aggregation mechanism is analogous to the optimization step in bundle adjustment, effectively refining camera parameters in a globally consistent manner while maintaining real-time inference efficiency.

Overall, the proposed streaming inference framework enables MoRe to achieve both efficiency and accuracy: causal attention ensures online processing capability, while the global token aggregation guarantees stable geometric reconstruction even in long sequences.

### 3.4. Training Objective

Following VGGT [39] and Dust3R [41], our training objective combines multi-task regression and classification, covering depth maps, point maps, camera parameters, and motion masks. For depth and point map regression, we adopt a confidence-weighted regression loss, which encourages

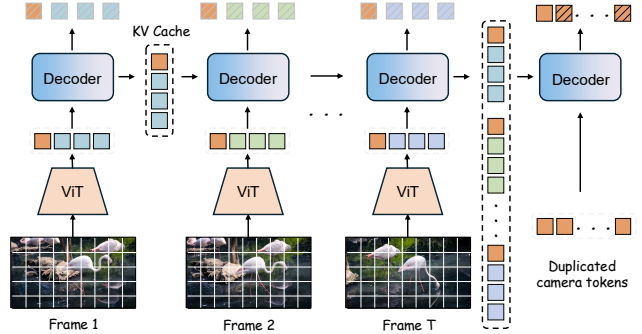


Figure 5. **Streaming Inference pipeline.** Leveraging causal attention, our model can efficiently process streaming input in an online manner. To enhance camera pose accuracy, we apply a bundle-adjustment-like post-processing step after the entire sequence has been processed. Specifically, for each frame, we duplicate the camera token and perform inference again using the previously cached key-value pairs.

both accurate predictions and reliable confidence estimates:

$$\mathcal{L}_{\text{conf}} = \sum_{i=1}^N \left( \hat{c}_i \|\hat{y}_i - y_i\|_2^2 - \lambda \log(\hat{c}_i) \right), \quad (6)$$

where  $N$  is the number of pixels or points,  $\hat{y}_i$  and  $y_i$  denote the predicted and ground-truth values respectively, and  $\hat{c}_i \in [1, \infty)$  represents the predicted confidence for each point.

For motion mask prediction, we employ a standard binary cross-entropy (BCE) loss, supervising each pixel to indicate whether it belongs to a dynamic region:

$$\mathcal{L}_{\text{motion}} = -\frac{1}{N} \sum_{i=1}^N \left[ M_i \log(\hat{M}_i) + (1 - M_i) \log(1 - \hat{M}_i) \right]. \quad (7)$$

As mentioned in Sec. 3.2, we encourage the camera token’s attention distribution over image tokens to align with the normalized motion scores. We use a simple confidence-like loss to enforce this alignment:

$$\mathcal{L}_{\text{attn}} = \frac{1}{M} \sum_{i=1}^M \max(0, a_i - C) \cdot \alpha_i. \quad (8)$$

where  $M$  is the number of image tokens and  $C$  is a constant to control the penalty region.

To enhance both the accuracy of the streaming predictions and the final grouped camera estimates, we adopt a training strategy that explicitly supervises the camera token in two parallel paths. During training, for each frame, we duplicate the camera token and move them to the end of the sequence. Both the original and the duplicated tokens are decoded to predict camera parameters, which are then compared to the ground truth. This encourages the model to maintain consistent predictions across both the streaming path and the post-hoc aggregation path.

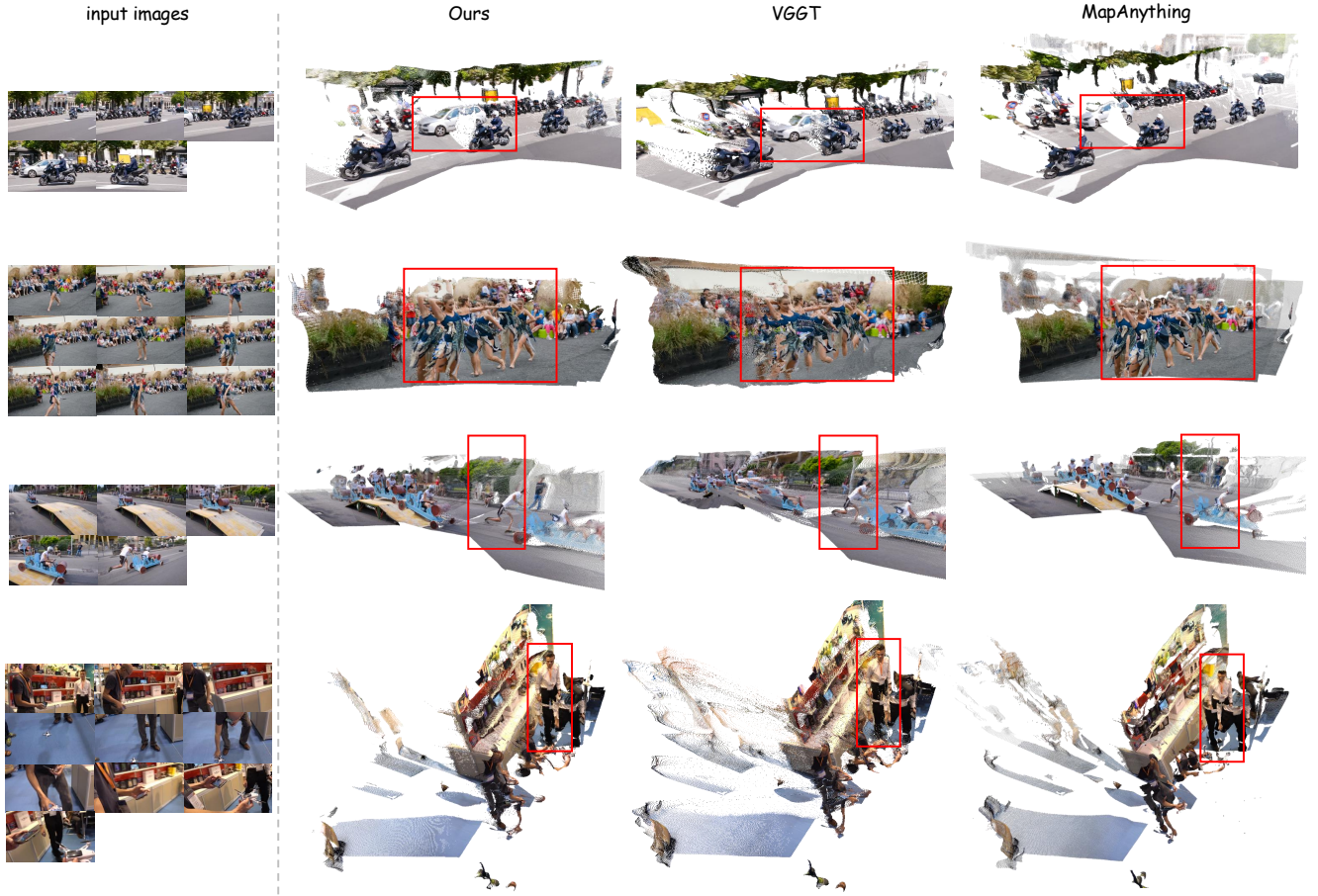


Figure 6. **Qualitative Comparison of Our Full Attention Model with Other Methods.** MoRe delivers outstanding performance in real-world scenes, outperforming other methods through its precise and robust geometry estimation.

Table 1. Camera Pose Estimation on Sintel [3], TUM-dynamics [33], Bonn [27], and ScanNet [5] datasets. FA refers to full attention.

| Method           | type      | Sintel        |                        |                      | Bonn          |                        |                      | TUM-dynamics  |                        |                      | ScanNet(static) |                        |                      |
|------------------|-----------|---------------|------------------------|----------------------|---------------|------------------------|----------------------|---------------|------------------------|----------------------|-----------------|------------------------|----------------------|
|                  |           | ATE↓          | RPE <sub>trans</sub> ↓ | RPE <sub>rot</sub> ↓ | ATE↓          | RPE <sub>trans</sub> ↓ | RPE <sub>rot</sub> ↓ | ATE↓          | RPE <sub>trans</sub> ↓ | RPE <sub>rot</sub> ↓ | ATE↓            | RPE <sub>trans</sub> ↓ | RPE <sub>rot</sub> ↓ |
| MapAnything [16] | FA        | 0.2104        | 0.0919                 | 2.7396               | 0.0248        | 0.0132                 | 0.6927               | 0.0244        | 0.0161                 | 0.3871               | 0.0603          | 0.0280                 | 0.8490               |
| VGGT [39]        | FA        | <u>0.1715</u> | <u>0.0617</u>          | <u>0.4695</u>        | <u>0.0141</u> | <u>0.0100</u>          | <u>0.6323</u>        | <b>0.0109</b> | <u>0.0092</u>          | <u>0.2992</u>        | <b>0.0347</b>   | <u>0.0151</u>          | <b>0.3758</b>        |
| MoRe(FA)         | FA        | <b>0.0877</b> | <b>0.0580</b>          | <b>0.3899</b>        | <b>0.0138</b> | <b>0.0099</b>          | <b>0.6267</b>        | <u>0.0115</u> | <b>0.0088</b>          | <b>0.2980</b>        | <u>0.0375</u>   | <b>0.0147</b>          | <u>0.3847</u>        |
| Spann3R [38]     | Streaming | 0.3313        | 0.1111                 | 4.4952               | 0.0344        | 0.0212                 | 2.2539               | 0.0421        | 0.0333                 | 0.8120               | 0.0651          | 0.0339                 | 0.9348               |
| CUT3R [40]       | Streaming | 0.2163        | <b>0.0756</b>          | <u>0.6518</u>        | 0.0420        | 0.0094                 | 0.6825               | 0.0438        | 0.0134                 | 0.4210               | 0.0929          | 0.0223                 | <u>0.5811</u>        |
| StreamVGGT [61]  | Streaming | 0.4159        | 0.1097                 | 1.1056               | 0.0451        | 0.0148                 | <b>0.5982</b>        | 0.0760        | 0.0317                 | 0.7012               | 0.1436          | 0.0437                 | 1.6533               |
| Wint3R [20]      | Streaming | 0.2251        | 0.0972                 | 1.0922               | 0.0366        | <b>0.0084</b>          | 0.7170               | 0.0700        | 0.0221                 | 0.7325               | 0.0618          | <b>0.0204</b>          | 0.7028               |
| Stream3R [17]    | Streaming | <u>0.2144</u> | <u>0.0764</u>          | 0.8674               | <u>0.0235</u> | <u>0.0108</u>          | 0.6664               | <b>0.0240</b> | <u>0.0123</u>          | <b>0.3180</b>        | <b>0.0521</b>   | 0.0215                 | 0.9919               |
| MoRe             | Streaming | <b>0.1474</b> | 0.0776                 | <b>0.6157</b>        | <b>0.0211</b> | 0.0117                 | <u>0.6496</u>        | <u>0.0260</u> | <b>0.0122</b>          | <u>0.3201</u>        | <u>0.0605</u>   | <u>0.0212</u>          | <b>0.5595</b>        |

As for specific supervision, we apply a relative supervision for each predicted pose pair. Formally, let  $S_{i \rightarrow j}$  denote the relative transform at time  $t$ .  $R_{i \rightarrow j}$  and  $t_{i \rightarrow j}$  respectively represents the rotation matrix and transform vector. The camera loss is defined as:

$$\mathcal{L}_{\text{cam}} = \frac{1}{T(T-1)} \sum_{i \neq j} (\theta_{\hat{R}_{i \rightarrow j}, R_{i \rightarrow j}} + \|\hat{t}_{i \rightarrow j} - t_{i \rightarrow j}\|), \quad (9)$$

where  $T$  is the total number of frames in the sequence.

Additionally, this loss is applied differently to the original and duplicated camera tokens. For the original camera tokens, when computing losses over relative transforms from earlier to later frames, gradients are detached for tokens from the earlier timestamps to prevent back-propagation through the entire temporal chain. In contrast, for the duplicated camera tokens, we retain full gradient flow across all temporal relations.

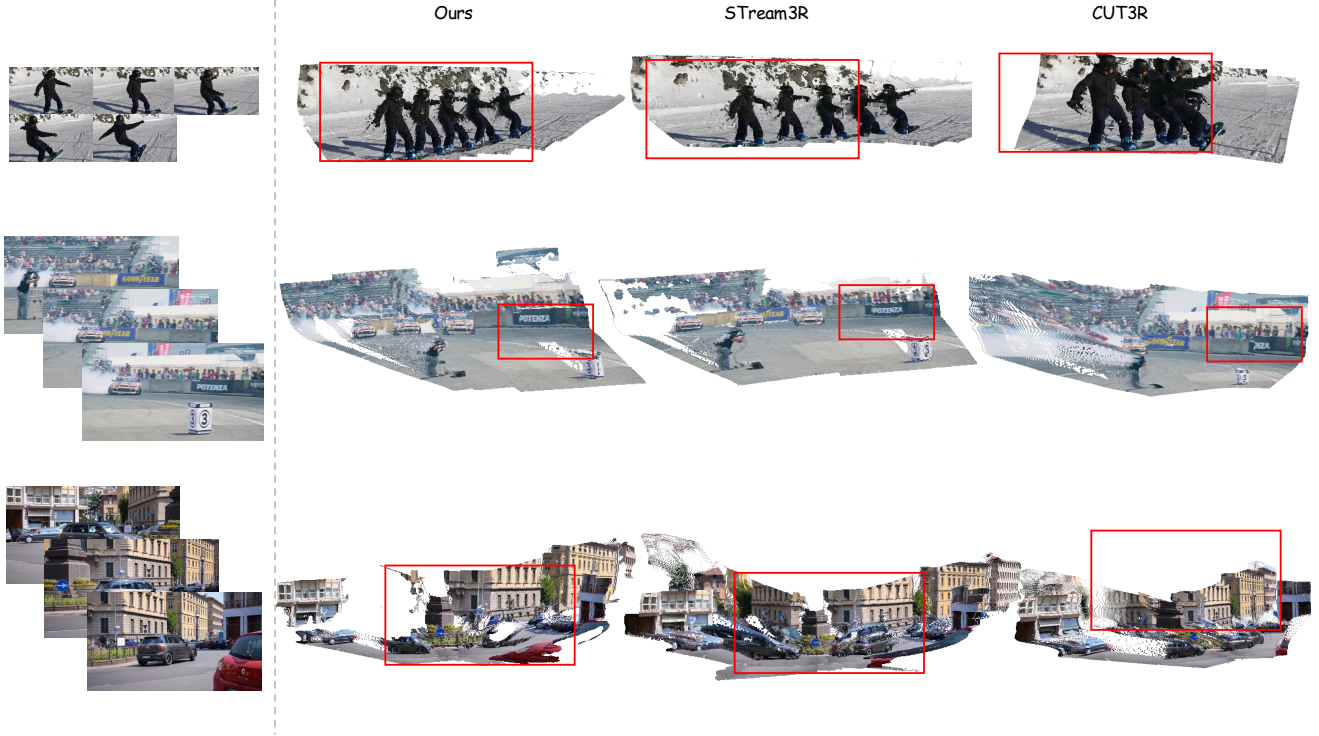


Figure 7. **Qualitative Comparison of our Stream Model with Other Methods.** MoRe strikes an optimal balance between reconstruction quality and computational efficiency, delivering high-fidelity results at competitive inference speeds.

## 4. Experiments

**Datasets.** Our model is trained on a large and diverse collection of datasets encompassing both static and dynamic scenes. Specifically, we utilize Dynamic Replica [15], PointOdyssey [56], Spring [23], Virtual KITTI [4], TartanAir [42], Co3Dv2 [30], ScanNet [5], BlendedMVS [49], Hypersim [31], ARKitScenes [1], Waymo [35], and OmniWorld-Game [60]. These datasets jointly cover a wide variety of indoor and outdoor environments, object categories, lighting conditions, and motion patterns. To ensure a balanced training distribution, datasets with fewer sequences are duplicated proportionally.

### 4.1. Camera Pose Estimation

Following previous works [17, 40], we evaluate our predicted camera poses on Sintel [3], TUM-dynamics [33], Bonn [27], and ScanNet [5]. The first three are dynamic datasets containing a large proportion of moving objects. Among them, TUM-dynamics and Bonn are real-world datasets with random camera jitter and complex motion patterns, posing significant challenges to static reconstruction methods. These properties make them ideal for evaluating camera pose estimation in 4D reconstruction scenarios. Notably, none of these dynamic datasets are seen during training, demonstrating the zero-shot generalization ability of our model. In contrast, ScanNet is a static in-

door dataset, which helps verify that our model not only performs well in dynamic 4D settings but also maintains strong capability on static reconstruction tasks. Our evaluation metrics include Absolute Translation Error (ATE), Relative Translation Error ( $RPE_{trans}$ ), and Relative Rotation Error ( $RPE_{rot}$ ), computed post Sim(3) alignment with ground truth poses. Quantitative results are summarized in Tab. 1. Among full-attention methods, our approach achieves comparable performance to the state-of-the-art  $\pi^3$  [44], despite being trained with significantly less data. Moreover, our method consistently outperforms streaming-based approaches, highlighting the effectiveness of our attention-forcing strategy in disentangling dynamic motion from static structure. This demonstrates that explicitly guiding attention during training leads to more robust and accurate camera pose estimation under challenging dynamic scenes.

### 4.2. Video Depth Estimation

We evaluate depth prediction on four widely used benchmarks, including Sintel, Bonn, TUM, and kitti, which collectively cover diverse scenarios, including both synthetic and real-world data, as well as indoor and outdoor environments. This provides a comprehensive evaluation of the model’s generalization ability across different domains. To quantify performance, we adopt standard metrics: the Absolute Relative Error (Abs-Rel), which measures the aver-

Table 2. Video Depth Estimation on Sintel [3], TUM-dynamics [33], Bonn [27] and kitti [12].

| Method           | type      | Sintel       |                          | Bonn         |                          | TUM-dynamics |                          | kitti        |                          |
|------------------|-----------|--------------|--------------------------|--------------|--------------------------|--------------|--------------------------|--------------|--------------------------|
|                  |           | Abs Rel↓     | $\delta < 1.25 \uparrow$ |
| Flare [52]       | FA        | 0.729        | 0.336                    | 0.116        | 0.897                    | 0.152        | 0.790                    | 0.356        | 0.570                    |
| MapAnything [16] | FA        | 0.632        | 0.461                    | 0.125        | 0.859                    | 0.241        | 0.813                    | 0.277        | 0.742                    |
| VGGT [39]        | FA        | <u>0.387</u> | <u>0.584</u>             | <b>0.055</b> | <u>0.970</u>             | <u>0.132</u> | <u>0.901</u>             | <u>0.073</u> | <u>0.961</u>             |
| MoRe(FA)         | FA        | <b>0.335</b> | <b>0.645</b>             | <b>0.055</b> | <b>0.971</b>             | <b>0.120</b> | <b>0.902</b>             | <b>0.066</b> | <b>0.967</b>             |
| Spann3R [38]     | Streaming | 0.740        | 0.364                    | 0.229        | 0.729                    | 0.264        | 0.645                    | 0.422        | 0.358                    |
| CUT3R [40]       | Streaming | 1.363        | 0.434                    | 0.076        | 0.949                    | 0.160        | 0.856                    | 0.124        | 0.873                    |
| StreamVGGT [61]  | Streaming | 0.698        | 0.591                    | 0.058        | <b>0.972</b>             | <u>0.156</u> | <u>0.889</u>             | 0.173        | 0.722                    |
| Wint3R [20]      | Streaming | 0.830        | 0.537                    | 0.071        | 0.912                    | 0.177        | 0.808                    | 0.201        | 0.601                    |
| Stream3R [17]    | Streaming | <u>0.397</u> | <u>0.632</u>             | <u>0.070</u> | 0.952                    | <b>0.151</b> | <b>0.898</b>             | <u>0.079</u> | <u>0.949</u>             |
| MoRe             | Streaming | <b>0.254</b> | <b>0.637</b>             | <b>0.068</b> | <u>0.961</u>             | 0.173        | 0.868                    | <b>0.072</b> | <b>0.966</b>             |

Table 3. Ablation on Camera Pose Estimation

| Method                 | Sintel       |                        |                      | TUM-dynamics |                        |                      |
|------------------------|--------------|------------------------|----------------------|--------------|------------------------|----------------------|
|                        | ATE↓         | RPE <sub>trans</sub> ↓ | RPE <sub>rot</sub> ↓ | ATE↓         | RPE <sub>trans</sub> ↓ | RPE <sub>rot</sub> ↓ |
| w/o attention forcing  | 0.163        | 0.092                  | 0.660                | 0.028        | 0.014                  | 0.329                |
| w/o BA-like refinement | 0.155        | 0.085                  | 0.619                | 0.027        | 0.014                  | 0.321                |
| full                   | <b>0.147</b> | <b>0.082</b>           | <b>0.616</b>         | <b>0.026</b> | <b>0.013</b>           | <b>0.320</b>         |

age proportional deviation between predicted and ground-truth depths, and  $\delta_{1.25}$  accuracy, representing the percentage of predictions within a multiplicative factor of 1.25 from the ground truth. Following prior works [17, 40], all predicted depth maps are aligned to the ground truth via a scale-only transformation before computing metrics. As shown in Tab. 2, our model achieves consistently strong results across all benchmarks. It performs competitively among full-attention methods and clearly surpasses existing streaming-based approaches, demonstrating its strong capability in monocular video depth estimation. Combined with the accurate camera pose estimation discussed earlier, these results validate that MoRe is well-suited for unified and robust 4D reconstruction.

### 4.3. Ablation Study

We perform ablation studies to investigate how different components of our model contribute to its overall performance. In particular, we examine the impact of the attention forcing mechanism, grouped causal attention and BA-like refinement under consistent training configurations.

**Attention Forcing** To validate of the proposed attention forcing strategy, we train two variants of our model: one with attention forcing and one without. Both models share the identical architecture, training schedule, and data configuration. We report their camera pose estimation results on the Sintel [3] and TUM-Dynamics [33] in Tab. 3. As shown in the table, introducing the attention forcing mechanism significantly improves the accuracy of camera pose estimation. This demonstrates that explicitly guiding the attention map toward static regions helps the model better disentangle dynamic motion from static structures.

Table 4. Ablation on Video Depth Estimation

| Method  | Sintel       |                          | Bonn         |                          | kitti        |                          |
|---------|--------------|--------------------------|--------------|--------------------------|--------------|--------------------------|
|         | Abs Rel↓     | $\delta < 1.25 \uparrow$ | Abs Rel↓     | $\delta < 1.25 \uparrow$ | Abs Rel↓     | $\delta < 1.25 \uparrow$ |
| w/o GCA | 0.277        | 0.592                    | 0.070        | 0.953                    | 0.079        | 0.949                    |
| w/      | <b>0.254</b> | <b>0.637</b>             | <b>0.068</b> | <b>0.961</b>             | <b>0.072</b> | <b>0.966</b>             |

**Grouped Causal Attention** To evaluate the effectiveness of our grouped causal attention, we compare it against a variant that adopts the standard causal attention for both training and inference. The baseline model is implemented with FlashAttention, and all other configurations are kept identical to ensure a fair comparison. We report depth estimation metrics on Sintel [3], Bonn [27] and kitti [12], as summarized in Tab. 4, where GCA refers to Grouped Causal Attention. Results show that our grouped causal attention consistently improves performance across datasets. This design enables each image token to attend to others within the same frame while maintaining causal temporal dependency, effectively enhancing both temporal reasoning and spatial consistency.

**BA-like refinement** We ablate the BA-like refinement by removing the duplicated camera tokens used for post-process refinement. Results on Sintel [3] and TUM-dynamics [33] are shown in Tab. 3. The variant without refinement shows noticeably higher translation and rotation errors, confirming that our BA-like refinement effectively improves pose accuracy and temporal consistency in streaming reconstruction.

## 5. Conclusion

We introduced MoRe, a feed-forward network for dynamic 4D reconstruction from monocular videos that effectively tackles challenges arising from moving objects and camera motion. By incorporating an attention-forcing strategy, MoRe explicitly disentangles dynamic motion from static scene geometry without requiring explicit motion priors during inference. Our streaming inference mechanism which combines grouped causal attention with a lightweight BA-like refinement, achieves efficient and temporally coherent reconstructions.

## References

- [1] Gilad Baruch, Zhuoyuan Chen, Afshin Dehghan, Tal Dimry, Yuri Feigin, Peter Fu, Thomas Gebauer, Brandon Joffe, Daniel Kurz, Arik Schwartz, et al. Arkitscenes: A diverse real-world dataset for 3d indoor scene understanding using mobile rgb-d data. *arXiv preprint arXiv:2111.08897*, 2021. 7
- [2] Tom Brown, Benjamin Mann, Nick Ryder, Melanie Subbiah, Jared D Kaplan, Prafulla Dhariwal, Arvind Neelakantan, Pranav Shyam, Girish Sastry, Amanda Askell, et al. Language models are few-shot learners. *Advances in neural information processing systems*, 33:1877–1901, 2020. 3
- [3] Daniel J Butler, Jonas Wulff, Garrett B Stanley, and Michael J Black. A naturalistic open source movie for optical flow evaluation. In *European conference on computer vision*, pages 611–625. Springer, 2012. 6, 7, 8
- [4] Yohann Cabon, Naila Murray, and Martin Humenberger. Virtual kitti 2. *arXiv preprint arXiv:2001.10773*, 2020. 7
- [5] Angela Dai, Angel X Chang, Manolis Savva, Maciej Halber, Thomas Funkhouser, and Matthias Nießner. Scannet: Richly-annotated 3d reconstructions of indoor scenes. In *Proceedings of the IEEE conference on computer vision and pattern recognition*, pages 5828–5839, 2017. 6, 7
- [6] Andrew J Davison, Ian D Reid, Nicholas D Molton, and Olivier Stasse. Monoslam: Real-time single camera slam. *IEEE transactions on pattern analysis and machine intelligence*, 29(6):1052–1067, 2007. 2
- [7] Yi Du, Zhipeng Zhao, Shaoshu Su, Sharath Golluri, Haoze Zheng, Runmao Yao, and Chen Wang. Superpc: a single diffusion model for point cloud completion, upsampling, denoising, and colorization. In *Proceedings of the Computer Vision and Pattern Recognition Conference*, pages 16953–16964, 2025. 2
- [8] Xianze Fang, Jingnan Gao, Zhe Wang, Zhuo Chen, Xingyu Ren, Jiangjing Lyu, Qiaomu Ren, Zhonglei Yang, Xiaokang Yang, Yichao Yan, and Chengfei Lyu. Dens3r: A foundation model for 3d geometry prediction. *arXiv preprint arXiv:2507.16290*, 2025. 2
- [9] Haiwen Feng, Junyi Zhang, Qianqian Wang, Yufei Ye, Pengcheng Yu, Michael J Black, Trevor Darrell, and Angjoo Kanazawa. St4rtrack: Simultaneous 4d reconstruction and tracking in the world. *arXiv preprint arXiv:2504.13152*, 2025. 2
- [10] Yasutaka Furukawa, Carlos Hernández, et al. Multi-view stereo: A tutorial. *Foundations and trends® in Computer Graphics and Vision*, 9(1-2):1–148, 2015. 2
- [11] Jingnan Gao, Zhe Wang, Xianze Fang, Xingyu Ren, Zhuo Chen, Shengqi Liu, Yuhao Cheng, Jiangjing Lyu, Xiaokang Yang, and Yichao Yan. More: 3d visual geometry reconstruction meets mixture-of-experts. *arXiv preprint arXiv:2510.27234*, 2025. 2
- [12] Andreas Geiger, Philip Lenz, Christoph Stiller, and Raquel Urtasun. Vision meets robotics: The kitti dataset. *The international journal of robotics research*, 32(11):1231–1237, 2013. 8, 2
- [13] Richard Hartley and Andrew Zisserman. *Multiple view geometry in computer vision*. Cambridge university press, 2003. 2
- [14] Linyi Jin, Richard Tucker, Zhengqi Li, David Fouhey, Noah Snavely, and Aleksander Holynski. Stereo4D: Learning How Things Move in 3D from Internet Stereo Videos. In *Proceedings of the IEEE/CVF Conference on Computer Vision and Pattern Recognition*, 2025. 2
- [15] Nikita Karaev, Ignacio Rocco, Benjamin Graham, Natalia Neverova, Andrea Vedaldi, and Christian Rupprecht. Dynamicstereo: Consistent dynamic depth from stereo videos. In *Proceedings of the IEEE/CVF Conference on Computer Vision and Pattern Recognition*, pages 13229–13239, 2023. 7
- [16] Nikhil Keetha, Norman Müller, Johannes Schönberger, Lorenzo Porzi, Yuchen Zhang, Tobias Fischer, Arno Knapitsch, Duncan Zauss, Ethan Weber, Nelson Antunes, et al. Mapanything: Universal feed-forward metric 3d reconstruction. *arXiv preprint arXiv:2509.13414*, 2025. 2, 6, 8
- [17] Yushi Lan, Yihang Luo, Fangzhou Hong, Shangchen Zhou, Honghua Chen, Zhaoyang Lyu, Shuai Yang, Bo Dai, Chen Change Loy, and Xingang Pan. Stream3r: Scalable sequential 3d reconstruction with causal transformer. *arXiv preprint arXiv:2508.10893*, 2025. 3, 6, 7, 8, 2
- [18] Vincent Leroy, Yohann Cabon, and Jérôme Revaud. Grounding image matching in 3d with mast3r. In *European Conference on Computer Vision*, pages 71–91. Springer, 2024. 3
- [19] Zhengqi Li, Richard Tucker, Forrester Cole, Qianqian Wang, Linyi Jin, Vickie Ye, Angjoo Kanazawa, Aleksander Holynski, and Noah Snavely. Megasam: Accurate, fast and robust structure and motion from casual dynamic videos. In *Proceedings of the Computer Vision and Pattern Recognition Conference*, pages 10486–10496, 2025. 2
- [20] Zizun Li, Jianjun Zhou, Yifan Wang, Haoyu Guo, Wenzheng Chang, Yang Zhou, Haoyi Zhu, Junyi Chen, Chunhua Shen, and Tong He. Wint3r: Window-based streaming reconstruction with camera token pool. *arXiv preprint arXiv:2509.05296*, 2025. 3, 6, 8
- [21] Ilya Loshchilov and Frank Hutter. Decoupled weight decay regularization. *arXiv preprint arXiv:1711.05101*, 2017. 1
- [22] Jiahao Lu, Tianyu Huang, Peng Li, Zhiyang Dou, Cheng Lin, Zhiming Cui, Zhen Dong, Sai-Kit Yeung, Wenping Wang, and Yuan Liu. Align3r: Aligned monocular depth estimation for dynamic videos. In *Proceedings of the Computer Vision and Pattern Recognition Conference*, pages 22820–22830, 2025. 2
- [23] Lukas Mehl, Jenny Schmalfluss, Azin Jahedi, Yaroslava Nalivayko, and Andrés Bruhn. Spring: A high-resolution high-detail dataset and benchmark for scene flow, optical flow and stereo. In *Proceedings of the IEEE/CVF Conference on Computer Vision and Pattern Recognition*, pages 4981–4991, 2023. 7
- [24] Richard A Newcombe, Dieter Fox, and Steven M Seitz. Dynamicfusion: Reconstruction and tracking of non-rigid scenes in real-time. In *Proceedings of the IEEE conference on computer vision and pattern recognition*, pages 343–352, 2015. 2

- [25] Zhenyu Ning, Jieru Zhao, Qihao Jin, Wenchao Ding, and Minyi Guo. Inf-mlm: Efficient streaming inference of multi-modal large language models on a single gpu. *arXiv preprint arXiv:2409.09086*, 2024. 1
- [26] Takeshi Noda, Chao Chen, Weiqi Zhang, Xinhai Liu, Yu-Shen Liu, and Zhizhong Han. Multipull: Detailing signed distance functions by pulling multi-level queries at multi-step. *Advances in Neural Information Processing Systems*, 37:13404–13429, 2024. 2
- [27] Emanuele Palazzolo, Jens Behley, Philipp Lottes, Philippe Giguere, and Cyrill Stachniss. Refusion: 3d reconstruction in dynamic environments for rgb-d cameras exploiting residuals. In *2019 IEEE/RSJ International Conference on Intelligent Robots and Systems (IROS)*, pages 7855–7862. IEEE, 2019. 6, 7, 8
- [28] Jordi Pont-Tuset, Federico Perazzi, Sergi Caelles, Pablo Arbeláez, Alex Sorkine-Hornung, and Luc Van Gool. The 2017 davis challenge on video object segmentation. *arXiv preprint arXiv:1704.00675*, 2017. 1, 3
- [29] Nikhila Ravi, Valentin Gabeur, Yuan-Ting Hu, Ronghang Hu, Chaitanya Ryali, Tengyu Ma, Haitham Khedr, Roman Rädle, Chloe Rolland, Laura Gustafson, et al. Sam 2: Segment anything in images and videos. *arXiv preprint arXiv:2408.00714*, 2024. 1
- [30] Jeremy Reizenstein, Roman Shapovalov, Philipp Henzler, Luca Sbordone, Patrick Labatut, and David Novotny. Common objects in 3d: Large-scale learning and evaluation of real-life 3d category reconstruction. In *Proceedings of the IEEE/CVF international conference on computer vision*, pages 10901–10911, 2021. 7, 3
- [31] Mike Roberts, Jason Ramapuram, Anurag Ranjan, Atulit Kumar, Miguel Angel Bautista, Nathan Paczan, Russ Webb, and Joshua M Susskind. Hypersim: A photorealistic synthetic dataset for holistic indoor scene understanding. In *Proceedings of the IEEE/CVF international conference on computer vision*, pages 10912–10922, 2021. 7
- [32] Johannes L Schonberger and Jan-Michael Frahm. Structure-from-motion revisited. In *Proceedings of the IEEE conference on computer vision and pattern recognition*, pages 4104–4113, 2016. 2
- [33] Jürgen Sturm, Nikolas Engelhard, Felix Endres, Wolfram Burgard, and Daniel Cremers. A benchmark for the evaluation of rgb-d slam systems. In *2012 IEEE/RSJ international conference on intelligent robots and systems*, pages 573–580. IEEE, 2012. 6, 7, 8
- [34] Edgar Sucar, Zihang Lai, Eldar Insafutdinov, and Andrea Vedaldi. Dynamic point maps: A versatile representation for dynamic 3d reconstruction. *arXiv preprint arXiv:2503.16318*, 2025. 2, 3
- [35] Pei Sun, Henrik Kretschmar, Xerxes Dotiwalla, Aurelien Chouard, Vijaysai Patnaik, Paul Tsui, James Guo, Yin Zhou, Yuning Chai, Benjamin Caine, et al. Scalability in perception for autonomous driving: Waymo open dataset. In *Proceedings of the IEEE/CVF conference on computer vision and pattern recognition*, pages 2446–2454, 2020. 7
- [36] Takafumi Taketomi, Hideaki Uchiyama, and Sei Ikeda. Visual slam algorithms: A survey from 2010 to 2016. *IPSA transactions on computer vision and applications*, 9(1):16, 2017. 2
- [37] Hugo Touvron, Thibaut Lavril, Gautier Izacard, Xavier Martinet, Marie-Anne Lachaux, Timothée Lacroix, Baptiste Rozière, Naman Goyal, Eric Hambro, Faisal Azhar, et al. Llama: Open and efficient foundation language models. *arXiv preprint arXiv:2302.13971*, 2023. 3, 1
- [38] Hengyi Wang and Lourdes Agapito. 3d reconstruction with spatial memory. *arXiv preprint arXiv:2408.16061*, 2024. 2, 6, 8
- [39] Jianyuan Wang, Minghao Chen, Nikita Karaev, Andrea Vedaldi, Christian Rupprecht, and David Novotny. Vggt: Visual geometry grounded transformer. In *Proceedings of the Computer Vision and Pattern Recognition Conference*, pages 5294–5306, 2025. 2, 3, 4, 5, 6, 8
- [40] Qianqian Wang, Yifei Zhang, Aleksander Holynski, Alexei A Efros, and Angjoo Kanazawa. Continuous 3d perception model with persistent state. In *Proceedings of the Computer Vision and Pattern Recognition Conference*, pages 10510–10522, 2025. 3, 6, 7, 8, 2
- [41] Shuzhe Wang, Vincent Leroy, Yohann Cabon, Boris Chidlovskii, and Jerome Revaud. Dust3r: Geometric 3d vision made easy. In *Proceedings of the IEEE/CVF Conference on Computer Vision and Pattern Recognition*, pages 20697–20709, 2024. 2, 5
- [42] Wenshan Wang, DeLong Zhu, Xiangwei Wang, Yaoyu Hu, Yuheng Qiu, Chen Wang, Yafei Hu, Ashish Kapoor, and Sebastian Scherer. Tartanair: A dataset to push the limits of visual slam. In *2020 IEEE/RSJ International Conference on Intelligent Robots and Systems (IROS)*, pages 4909–4916. IEEE, 2020. 7
- [43] Yihan Wang, Lahav Lipson, and Jia Deng. Sea-raft: Simple, efficient, accurate raft for optical flow. In *European Conference on Computer Vision*, pages 36–54. Springer, 2024. 1
- [44] Yifan Wang, Jianjun Zhou, Haoyi Zhu, Wenzheng Chang, Yang Zhou, Zizun Li, Junyi Chen, Jiangmiao Pang, Chunhua Shen, and Tong He.  $\pi^3$ : Permutation-equivariant visual geometry learning. *arXiv preprint arXiv:2507.13347*, 2025. 7, 3
- [45] Guangxuan Xiao, Yuandong Tian, Beidi Chen, Song Han, and Mike Lewis. Efficient streaming language models with attention sinks. *arXiv preprint arXiv:2309.17453*, 2023. 1
- [46] Jianing Yang, Alexander Sax, Kevin J Liang, Mikael Henaff, Hao Tang, Ang Cao, Joyce Chai, Franziska Meier, and Matt Feiszli. Fast3r: Towards 3d reconstruction of 1000+ images in one forward pass. In *Proceedings of the Computer Vision and Pattern Recognition Conference*, pages 21924–21935, 2025. 2, 3
- [47] David Yifan Yao, Albert J Zhai, and Shenlong Wang. Uni4d: Unifying visual foundation models for 4d modeling from a single video. In *Proceedings of the Computer Vision and Pattern Recognition Conference*, pages 1116–1126, 2025. 2
- [48] Runmao Yao, Junsheng Zhou, Zhen Dong, and Yu-Shen Liu. Anchoredream: Zero-shot 360° indoor scene generation from a single view via geometric grounding, 2026. 2
- [49] Yao Yao, Zixin Luo, Shiwei Li, Jingyang Zhang, Yufan Ren, Lei Zhou, Tian Fang, and Long Quan. Blendedmvs: A large-scale dataset for generalized multi-view stereo networks. In

- Proceedings of the IEEE/CVF conference on computer vision and pattern recognition*, pages 1790–1799, 2020. 7
- [50] Junyi Zhang, Charles Herrmann, Junhwa Hur, Varun Jampani, Trevor Darrell, Forrester Cole, Deqing Sun, and Ming-Hsuan Yang. Monst3r: A simple approach for estimating geometry in the presence of motion. *arXiv preprint arXiv:2410.03825*, 2024. 2
- [51] Songyan Zhang, Yongtao Ge, Jinyuan Tian, Guangkai Xu, Hao Chen, Chen Lv, and Chunhua Shen. Pomato: Marrying pointmap matching with temporal motion for dynamic 3d reconstruction. *arXiv preprint arXiv:2504.05692*, 2025. 2
- [52] Shangzhan Zhang, Jianyuan Wang, Yinghao Xu, Nan Xue, Christian Rupprecht, Xiaowei Zhou, Yujun Shen, and Gordon Wetzstein. Flare: Feed-forward geometry, appearance and camera estimation from uncalibrated sparse views. In *Proceedings of the Computer Vision and Pattern Recognition Conference*, pages 21936–21947, 2025. 8, 3
- [53] Wenyuan Zhang, Jimin Tang, Weiqi Zhang, Yi Fang, Yu-Shen Liu, and Zhizhong Han. Materialrefgs: Reflective gaussian splatting with multi-view consistent material inference. *arXiv preprint arXiv:2510.11387*, 2025. 2
- [54] Weiqi Zhang, Junsheng Zhou, Haotian Geng, Wenyuan Zhang, and Yu-Shen Liu. Gap: Gaussianize any point clouds with text guidance. In *Proceedings of the IEEE/CVF International Conference on Computer Vision (ICCV)*, pages 25627–25638, 2025. 2
- [55] Weiqi Zhang, Junsheng Zhou, Haotian Geng, Kanle Shi, Yi Fang, and Yu-Shen Liu. Gaussiangrow: Geometry-aware gaussian growing from 3d point clouds with text guidance. In *Proceedings of the IEEE/CVF Conference on Computer Vision and Pattern Recognition (CVPR)*, 2026. 2
- [56] Yang Zheng, Adam W Harley, Bokui Shen, Gordon Wetzstein, and Leonidas J Guibas. Pointodyssey: A large-scale synthetic dataset for long-term point tracking. In *Proceedings of the IEEE/CVF International Conference on Computer Vision*, pages 19855–19865, 2023. 7
- [57] Junsheng Zhou, Weiqi Zhang, and Yu-Shen Liu. Diffgs: Functional gaussian splatting diffusion. In *Advances in Neural Information Processing Systems*, pages 37535–37560. Curran Associates, Inc., 2024. 2
- [58] Junsheng Zhou, Weiqi Zhang, Baorui Ma, Kanle Shi, Yu-Shen Liu, and Zhizhong Han. Udiff: Generating conditional unsigned distance fields with optimal wavelet diffusion. In *Proceedings of the IEEE/CVF Conference on Computer Vision and Pattern Recognition (CVPR)*, pages 21496–21506, 2024. 2
- [59] Junsheng Zhou, Weiqi Zhang, Baorui Ma, Kanle Shi, Yu-Shen Liu, and Zhizhong Han. Udfstudio: A unified framework of datasets, benchmarks and generative models for unsigned distance functions. *IEEE Transactions on Pattern Analysis and Machine Intelligence*, 2026. 2
- [60] Yang Zhou, Yifan Wang, Jianjun Zhou, Wenzheng Chang, Haoyu Guo, Zizun Li, Kaijing Ma, Xinyue Li, Yating Wang, Haoyi Zhu, et al. Omniworld: A multi-domain and multi-modal dataset for 4d world modeling. *arXiv preprint arXiv:2509.12201*, 2025. 7
- [61] Dong Zhuo, Wenzhao Zheng, Jiahe Guo, Yuqi Wu, Jie Zhou, and Jiwen Lu. Streaming 4d visual geometry transformer. *arXiv preprint arXiv:2507.11539*, 2025. 3, 6, 8

# MoRe: Motion-aware Feed-forward 4D Reconstruction Transformer

## Supplementary Material

### 6. Training Details

We train our model using the AdamW optimizer [21] to minimize the overall loss function. The training is conducted for 100K iterations with a learning rate scheduler that includes a warm-up phase and a peak learning rate of  $1 \times 10^{-6}$ . At each iteration, we randomly sample 2–24 frames from each sequence with a temporal interval of 1–5. The input images are resized such that the longer side is fixed to 518 pixels, while the shorter side is randomly scaled by a factor of 0.8–1.2 for data augmentation. Training is performed on 64 NVIDIA A800 GPUs for approximately two days. We adopt bfloat16 precision and gradient checkpointing to reduce memory consumption and enable efficient large-scale training.

### 7. Motion Mask Extraction

#### 7.1. Data Preparation

Most existing datasets lack reliable motion-mask annotations, making it difficult to obtain high-quality supervision for dynamic scene understanding. To address this issue, we propose a robust motion-mask extraction pipeline. Given raw images, we first apply SAM2 [29] to obtain semantic segmentation masks. The ego flow is computed from ground-truth camera poses and intrinsics, while SEARAFT [43] predicts the optical flow.

For each semantic region  $S_k$ , we compute the average flow discrepancy:

$$d_k = \frac{1}{|S_k|} \sum_{(i,j) \in S_k} \|\mathbf{F}^{\text{pred}}(i,j) - \mathbf{F}^{\text{ego}}(i,j)\|_2. \quad (10)$$

A semantic region is considered moving if its discrepancy exceeds a statistical threshold:

$$d_k > \mu_d + 2\sigma_d. \quad (11)$$

Finally, the motion mask  $M(u, v)$  is defined as:

$$M(u, v) = \begin{cases} 1, & \text{if } (u, v) \in S_k \text{ and } d_k > \mu_d + 2\sigma_d, \\ 0, & \text{otherwise.} \end{cases} \quad (12)$$

#### 7.2. Qualitative Results

We evaluate our method on the DAVIS [28] dataset. For visualization, we present both the raw outputs of our model and a refined version obtained by applying the image-level predictor of SAM2 [29]. As shown in Fig. 8, our approach

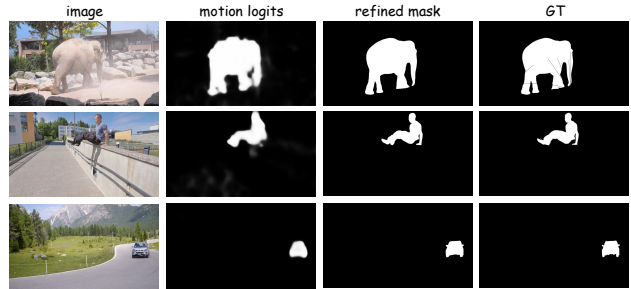


Figure 8. **Qualitative Results of Motion Mask Extraction.** Our method robustly captures moving objects across diverse scenes and objects.

consistently produces accurate motion-object segmentation across diverse scenes and object categories. After simple post-processing, the generated motion masks are sufficiently clean and robust to be directly used in downstream tasks such as dynamic scene reconstruction, moving-object removal, and motion-aware 4D generation.

### 8. Stream Inference

#### 8.1. Implementation Details

Streaming generation has been widely adopted in large language models and related multi-modal systems to reduce latency and computational cost [25, 37, 45]. Inspired by this paradigm, we introduce streaming and causal attention mechanisms into MoRe, enabling real-time, constant-latency generation with image-wise KV caching. This design effectively avoids redundant computation by reusing the stored key-value pairs from previous steps. In addition, we incorporate a window-sliding strategy to prevent unbounded growth of the KV cache.

We employ two streamers: an input streamer for continuous image ingestion and an output streamer for delivering predictions. In the work flow, each new image enters an infinite decoding loop, where its hidden states are concatenated with cached keys and values – optionally applying window sliding – before passing through the stack of N transformer layers. The updated prediction is then immediately emitted through the output streamer, enabling continuous and low-latency streaming outputs.

#### 8.2. Efficiency Test

We evaluate the inference speed of our method on the KITTI dataset at a resolution of 512×144 using an NVIDIA A800 GPU, ensuring consistency across all compared approaches

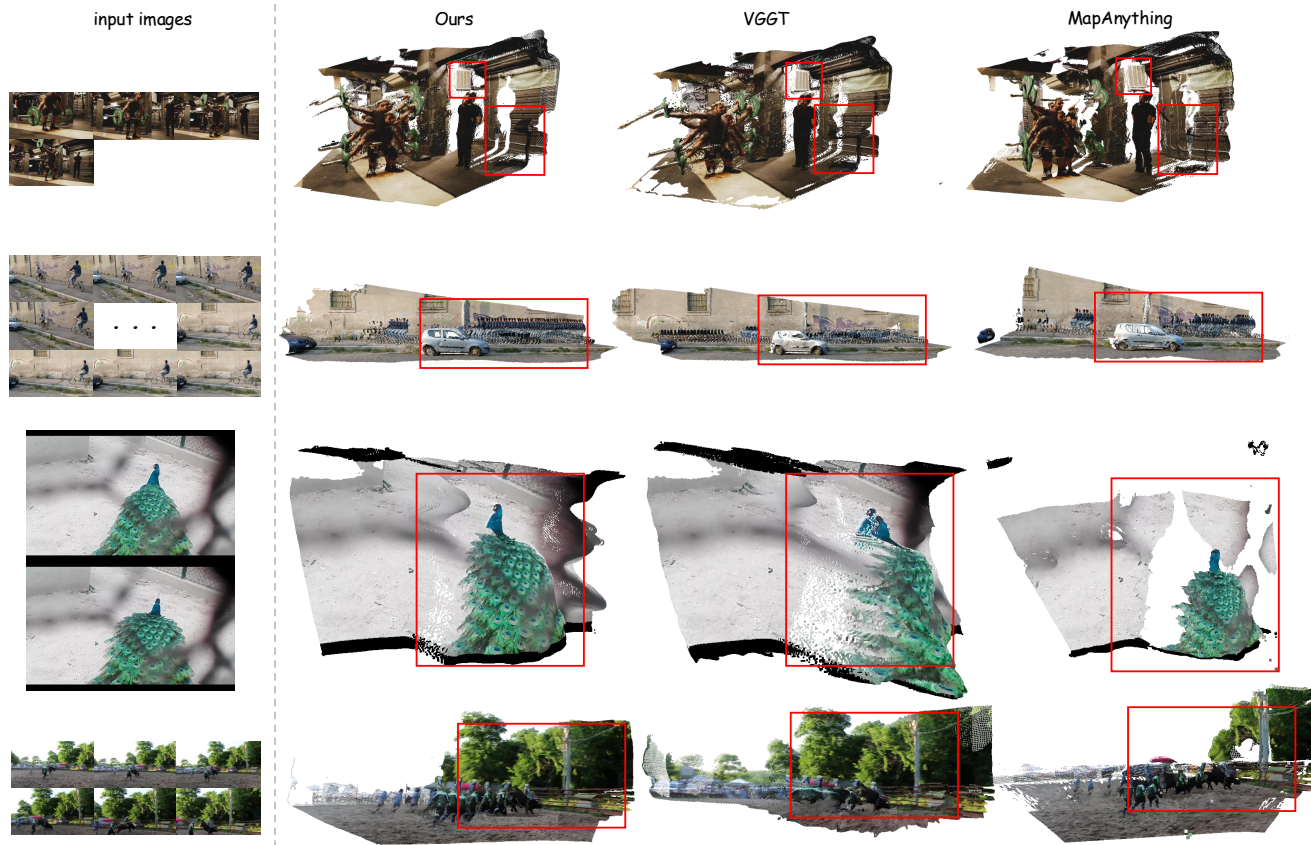


Figure 9. **Qualitative Comparison of Our Model with Other Methods.** We present an extensive set of visual results showcasing reconstruction quality, motion handling, and robustness under challenging dynamic scenarios.

Table 5. Inference speed comparison (FPS), tested on KITTI [12].

| Method                                      | FPS   |
|---|-------|
| VGGT [39]                                   | 7.32  |
| Spann3R [38] (224×224)                      | 13.55 |
| CUT3R [40]                                  | 16.58 |
| Stream3R <sup>α</sup> [17]                  | 23.48 |
| Stream3R <sup>β</sup> [17]                  | 12.95 |
| Stream3R <sup>β</sup> -W[5] [17] (window=5) | 32.93 |
| MoRe  | 30.09 |

except for Spann3R [38], which processes Stream inputs at a resolution of 224×224. The performance of other baselines follows the Stream3R [17] evaluation results. In addition, we report the FPS of our model employing a sliding window attention mechanism with a window size of 5. As shown in Tab. 5, our method achieves inference speeds within the fastest tier among all evaluated methods, outperforming most baselines while maintaining competitive reconstruction accuracy. This demonstrates that our approach

provides an excellent trade-off between speed and performance, making it highly suitable for real-time 4D reconstruction systems and applications.

### 8.3. Qualitative Results

To qualitatively evaluate the reconstruction quality of our approach, we further visualize the dynamic 4D scenes reconstructed from monocular video sequences. As shown in Fig. 9, our method effectively captures both static scene geometry and dynamic object motion with high fidelity and temporal coherence. The detailed geometry and consistent motion trajectories demonstrate the robustness of our model in handling complex dynamic environments. These visual results further validate the effectiveness of our approach for practical 4D reconstruction applications. In addition to the stream inference, we also provide more examples of the full attention model. For some methods, slight deviations in the rendered viewpoint occur because their reconstructed point clouds have different scales.

Table 6. Camera Pose Estimation Comparison on Co3Dv2 [30].

| Method       | Co3Dv2       |              |              |
|--------------|--------------|--------------|--------------|
|              | RRA@30↑      | RTA@30↑      | AUC@30↑      |
| Fast3R [46]  | 97.49        | 91.11        | 73.43        |
| CUT3R [40]   | 96.19        | 92.69        | 75.82        |
| FLARE [52]   | 96.38        | 93.76        | 73.99        |
| VGGT [39]    | 98.96        | 97.13        | 88.59        |
| $\pi^3$ [44] | 99.05        | 97.33        | 88.41        |
| MoRe         | <b>99.49</b> | <b>98.11</b> | <b>91.42</b> |

## 9. Motion Aligned Attention

### 9.1. Quantitative Results

We further evaluate our model on the Co3Dv2 [30] dataset to verify its capability in static scene reconstruction, and we additionally compare against a broader range of baselines. The results are summarized in Tab. 6. As discussed in the main text, our full-attention variant achieves the best overall performance and surpasses all baselines, including the state-of-the-art  $\pi^3$  method. These results demonstrate that, although our architecture and training strategy are primarily designed for modeling dynamic scenes and suppressing motion-induced ambiguities, the model retains excellent reconstruction accuracy on purely static scenarios. This highlights the strong robustness and generalization ability of our approach: the motion-aware design does not compromise performance when no motion is present, and instead enables the model to effectively capture both dynamic and static structural cues in a unified framework.

### 9.2. Visualization

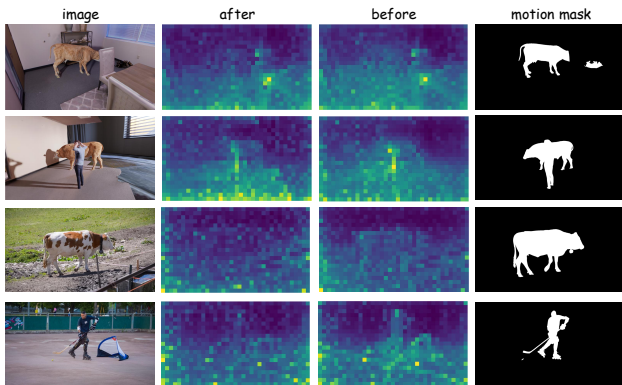


Figure 10. **Attention Map Comparison.** We visualize the attention map on Dynamic Replica [34] and DAVIS [28] dataset. Our motion-aligned training suppresses undesired attention from camera tokens to dynamic objects, yielding cleaner and more structured attention patterns.

To better illustrate the effectiveness of our motion-aligned training strategy, we visualize and compare the attention weight maps of camera token before and after training. Specifically, we select the last attention layer of our model and compute the average attention weight across all heads to obtain a stable and interpretable heatmap representation. As shown in Fig. 10, the attention distribution becomes significantly more structured. The attention weight from camera tokens to dynamic objects is notably suppressed, while attention toward static regions becomes more concentrated and semantically coherent. This indicates that the model has learned to reserve camera tokens for representing stable scene information, preventing dynamic content from leaking into the global representation. The resulting separation leads to cleaner latent features, more stable motion reasoning, and ultimately more accurate 4D reconstruction. These observations validate that our training strategy effectively regularizes the attention behavior and enforces the intended representational roles of different token types.

### 9.3. Loss Design

We initially explored divergence-based formulations, such as applying a KL divergence to align the attention distribution to the motion-score distribution. While this approach appears principled, it implicitly normalizes attention into a probability distribution, which tends to introduce an undesirable inductive bias in static scenes. In static regions, the correct behavior should allow attention weights to remain largely unconstrained, whereas KL-based losses force all tokens to contribute to a normalized distribution even when no motion exists, leading to degraded performance. The constant  $C$  serves as a neutral baseline representing the default attention level. During training, tokens with high motion scores ( $\hat{\alpha}_i$  large) are encouraged to deviate from this baseline, while tokens associated with static content ( $\hat{\alpha}_i \approx 0$ ) receive minimal gradient updates. This yields a motion-adaptive behavior that avoids imposing constraints where no motion is present. The multiplicative term  $(\alpha_i - C) \hat{\alpha}_i$  acts as a gating mechanism, in which motion-relevant tokens receive stronger supervision and motion-irrelevant tokens are softly ignored. This formulation provides flexibility and avoids the normalization issues inherent to divergence losses. We conducted ablations comparing the proposed loss with a KL-based alternative. As shown in Tab. 7, the KL formulation performs worse in both static and low-motion scenarios, confirming that the proposed motion-gated design better matches the nature of the task and provides more stable training behavior.

Table 7. Ablation on Loss Function for Motion Alignment.

| Method     | Sintel           |                                 |                               | TUM-dynamics     |                                 |                               |
|------------|------------------|---------------------------------|-------------------------------|------------------|---------------------------------|-------------------------------|
|            | ATE $\downarrow$ | RPE $_{\text{trans}}\downarrow$ | RPE $_{\text{rot}}\downarrow$ | ATE $\downarrow$ | RPE $_{\text{trans}}\downarrow$ | RPE $_{\text{rot}}\downarrow$ |
| w/ KL loss | 0.185            | 0.084                           | 0.707                         | 0.029            | 0.015                           | 0.350                         |
| Ours       | <b>0.147</b>     | <b>0.082</b>                    | <b>0.616</b>                  | <b>0.026</b>     | <b>0.013</b>                    | <b>0.320</b>                  |

## 10. Limitations

Despite demonstrating strong performance in dynamic scenes, our method has several limitations. First, although our method achieves strong results in dynamic scene modeling, it heavily depends on the accuracy and quality of motion mask annotations. Since the motion masks provide critical supervision to distinguish moving regions from static background, any errors, noise, or inconsistencies in these masks can propagate through the training process, leading to degraded reconstruction quality and less reliable motion reasoning. This reliance poses a limitation, especially when high-quality motion mask labels are unavailable or difficult to obtain in real-world scenarios. Future work could explore more robust or self-supervised techniques to mitigate the impact of imperfect motion supervision and reduce dependency on manual or heuristic mask extraction. Second, while the feed-forward architecture enables efficient and real-time inference, it may struggle to capture very long-term temporal dependencies and complex dynamic interactions that extend beyond the modeled temporal window. Third, the model may exhibit reduced robustness in scenes with extremely fast or non-rigid motions, where motion patterns are highly irregular and difficult to disentangle. In addition, our model can fail in heavily motion-blurred scenarios, where rapid camera movement or fast object motion leads to severely degraded visual cues. In such cases, attention alignment becomes unreliable, causing inaccurate depth, unstable poses, or distorted geometry. Lastly, our current approach does not explicitly handle occlusions or severe appearance changes over time, which can lead to artifacts or inconsistencies in the reconstructed 4D scenes. Addressing these challenges is an important direction for future research.